DØ Note 5871-CONF

Search for Higgs Boson Production in Dilepton plus Missing Transverse Energy Final States with 3.0–4.2 fb^{-1} of $p\overline{p}$ Collisions at $\sqrt{s} = 1.96$ TeV

The DØ Collaboration
URL http://www-d0.fnal.gov
(Dated: March 6, 2009)

A search for the standard model (SM) Higgs boson is presented using a sample of dilepton events with large missing transverse momentum extracted from 3.0–4.2 fb^{-1} of $p\overline{p}$ collisions at $\sqrt{s} = 1.96$ TeV. Final states containing either e^+e^-, $e^\pm\mu^\mp$, or $\mu^+\mu^-$ are considered. The data sample used in this analysis was collected between April 2002 and December 2008 by the DØ detector during Run II of the Fermilab Tevatron collider. No significant excess above background estimations is observed, and upper limits on Higgs boson production are derived, which are 1.2 times the expected SM cross section at M_H=170 GeV.

Preliminary Results for Winter Conferences 2009

I. INTRODUCTION

In the standard model (SM) the masses of the charged fermions are generated by their interaction with a scalar field, the Higgs boson, which has yet to be observed experimentally. The Higgs boson represents the residual degree of freedom after the spontaneous symmetry breaking of the electroweak gauge symmetry $\mathcal{SU}(2) \otimes \mathcal{U}(1)$ which is responsible for the generation of the masses of the W and Z bosons. Direct searches at the CERN e^+e^- collider (LEP) yield a lower limit for the SM Higgs boson mass, $M_H > 114.4$ GeV [1] at 95% confidence level (C.L.). Indirect measurements via fits to the electroweak precision data give an upper bound of $M_H < 185$ GeV [2] at 95% C.L. when combined with the direct searches.

In this note we present a search for the Higgs boson in final states containing two reconstructed leptons and missing transverse energy ($\not\!\!E_T$), using data collected with the DØ detector at the Fermilab Tevatron corresponding to an integrated luminosity of 3.0–4.2 fb^{-1}. We consider final states containing either two reconstructed electrons, e^+e^-, an electron and a muon, $e^\pm\mu^\mp$, or two muons, $\mu^+\mu^-$. Final states with tau leptons are detected through the tau leptonic decay modes to electrons or muons, or final states which leave an electron-like signal in the detector. Together these final states provide the largest sensitivity for the SM Higgs boson at the Tevatron for $M_H \sim 160$ GeV [3, 4]. The search presented in this note considers not only the contribution to the dilepton plus $\not\!\!E_T$ final state from the $H \to WW^{(*)} \to \ell\ell'\nu\nu$ $(\ell, \ell' = e, \mu, \tau)$ decay where the Higgs boson is produced through the gluon fusion process, but also contributions from the weak boson fusion process. In addition we also consider final states originating from Higgs boson production in association with a vector boson (WH or ZH), where leptons may originate from the vector boson or Higgs boson decay, excluding events which are considered in the Higgs search in the $Wb\bar{b}$ and $Zb\bar{b}$ final states. Results are presented relative to the sum of the SM predictions for the cross sections of the different Higgs boson production processes, assuming the SM values for the Higgs branching fractions. The limits on Higgs boson production obtained in this analysis supersede previous DØ results presented in [5, 6].

II. DØ DETECTOR

We briefly describe the main components of the DØ Run II detector [7] relevant to this analysis. The central tracking system consists of a silicon microstrip tracker (SMT) and a central fiber tracker (CFT), both located within a 2 T axial magnetic field. The SMT strips have a typical pitch of 50–80 μm, and the design is optimized for tracking and vertexing over the pseudorapidity range $|\eta| < 3$, where $\eta = -\ln(\tan\theta/2)$ with θ being the polar angle relative to the proton beam direction. The system has a six-barrel longitudinal structure, with each barrel a set of four silicon layers arranged axially around the beam pipe, interspersed with sixteen radial disks. In addition, a new layer of silicon (Layer 0) was added just outside the beam pipe in 2006. The CFT has eight thin coaxial barrels, each supporting two doublets of overlapping scintillating fibers of 0.835 mm diameter, one doublet parallel to the beam axis, the other alternating by $\pm 3^\circ$ relative to the beam axis.

A liquid-argon/uranium calorimeter surrounds the central tracking system and consists of a central calorimeter (CC) covering to $|\eta| \approx 1.1$, and two end calorimeters (EC) extending coverage for $|\eta| < 4.2$, each housed in separate cryostats. Scintillators between the CC and EC cryostats provide sampling of showers for $1.1 < |\eta| < 1.4$.

The muon system is located outside the calorimeters and consists of a layer of tracking detectors and scintillation trigger counters inside toroid magnets which provide a 1.8 T magnetic field, followed by two similar layers behind each toroid. Tracking in the muon system for $|\eta| < 1$ relies on 10 cm wide drift tubes, while 1 cm mini-drift tubes are used for $1 < |\eta| < 2$.

Trigger and data acquisition systems are designed to accommodate the high luminosities of Run II. Based on preliminary information from tracking, calorimetry, and muon systems, the output of the first level of the trigger is used to limit the rate for accepted events to ≈ 1.5 kHz. At the next trigger stage, with more refined information, the rate is reduced further to ≈ 0.8 kHz. These first two levels of triggering rely mainly on hardware and firmware. The third and final level of the trigger, with access to all the event information, uses software algorithms and a computing farm, and reduces the output rate to ≈ 100 Hz, which is written to tape.

III. DATA AND MONTE CARLO SAMPLES

The data sample used in this analysis was collected between April 2002 and December 2008 (Run II) by the DØ detector at the Fermilab Tevatron collider at $\sqrt{s} = 1.96$ TeV, and corresponds to an integrated luminosity of 3.0 fb^{-1} for the $\mu^+\mu^-$ final state and of 4.2 fb^{-1} for the e^+e^- and $e^\pm\mu^\mp$ final states. The luminosity is measured with an accuracy of 6.1% using plastic scintillator arrays located in front of the EC cryostats, covering $2.7 < |\eta| < 4.4$ [8].

As a cross–check the integrated luminosity is compared with the number of observed Z events in the mass region $60< M_{\ell\ell} <130$ GeV and the NNLO $Z/\gamma^* \to ee$ $(\mu\mu)$ cross section, after applying all known correction factors to the Monte Carlo (MC) simulation in order to reproduce the efficiencies measured in data (for the $e^{\pm}\mu^{\mp}$ final state the entire $M_{e\mu}$ spectrum is used considering the effect of the τ branching ratios). The yield of Z candidates observed in data is consistent with the measurement of the luminosity within 5%.

Signal and SM background processes are simulated with PYTHIA [9] using the CTEQ6L1 [10] parton distribution functions (PDF), followed by a detailed GEANT-based [11] simulation of the DØ detector. Various Higgs boson production channels contribute to the total signal. The main production channel is the gluon fusion process $gg \to H \to WW^* \to \ell\nu\ell\nu$, followed by the the vector–boson fusion process (VBF) $q\bar{q} \to q\bar{q}H \to qqWW^* \to \ell\nu\ell\nu$. Smaller additional signal contributions come from ZH and WH production. The signal cross sections are normalized to NNLO calculations [12–15] (NLO calculations in the case of the vector boson fusion process) and the distribution of the transverse momentum of the Higgs boson generated in the gluon fusion process is reweighted to match the SHERPA simulation [16].

The main background processes for this analysis are diboson production, Z decays in leptonic final states, electroweak $W + jet/\gamma$ production, $t\bar{t}$ decays and multijet production with misidentified leptons. For the W(+jets) background we use the ALPGEN [17] event generator (PYTHIA is used for the $\mu^+\mu^-$ final state). The background MC samples for inclusive W and Z production are normalized using the NNLO cross sections calculations of [18] using the NLO CTEQ 6.1 PDF. The Z boson $p_{\rm T}$ distribution is modeled to match the distribution observed in data [19], taking also into account the dependence on the number of reconstructed jets (for simplicity PYTHIA is used for generating the Z+jets background instead of ALPGEN). The NNLO calculations of [20] are used for $t\bar{t}$ production, while the NLO WW, WZ and ZZ production cross section values are taken from [21]. For the main source of background, WW production, the $p_{\rm T}$ of the diboson system is modeled using the SHERPA simulation and the distribution of the opening angle of the two leptons is corrected to take into account the contribution from gluon fusion [22].

The background due to multijet production, when jets are misidentified as leptons, is determined from data. A sample of like-sign dilepton events is used in the $\mu\mu$ channel, corrected for like-sign contributions from other processes. The other channels use events with inverted lepton quality cuts, corrected to match the normalization and kinematics determined in the like-sign data.

IV. EVENT SELECTION

The $H \to WW^{(*)} \to \ell\ell'$ $(\ell, \ell' = e, \mu, \tau)$ candidates are selected by triggering on single or dilepton events using a three level trigger system. The first trigger level uses hardware to select electron candidates based on energy deposition in the electromagnetic part of the calorimeter and muon candidates formed by hits in the muon system. The muon trigger requires in addition a high $p_{\rm T}$ central track reconstructed in the CFT by the specialized central track trigger (CTT). Digital signal processors in the second trigger level form muon track candidate segments defined by hits in the muon drift chambers and scintillators, as well as match lepton candidates to a more precise central track using additional SMT hits reconstructed by the silicon track trigger. At the third level, software algorithms running on a computing farm and exploiting the full event information are used to make the final selection of events which are recorded.

In the offline analysis, electrons are identified using calorimeter and tracking information. Electromagnetic showers are identified in the calorimeter by comparing the longitudinal and transverse shower profiles to those of simulated electrons. The showers must be isolated, deposit most of their energy in the electromagnetic part of the calorimeter and pass a likelihood criterion that includes a spatial track match and, in the central detector region, an E/p requirement, where E is the energy of the calorimeter cluster and p is the momentum of the track. Electrons must be reconstructed within a detector pseudorapidity $|\eta| < 3.0$. The transverse momentum measurement of the electrons is based on calorimeter cell energy information.

Muon tracks are reconstructed from hits in the wire chambers and scintillators in the muon system and must match a track in the central tracker. To select isolated muons, the scalar sum of the transverse momentum of all tracks, other than that of the muon, in a cone of $\mathcal{R} = 0.5$ around the muon track is calculated, where $\mathcal{R} = \sqrt{(\Delta\phi)^2 + (\Delta\eta)^2}$ and ϕ is the azimuthal angle. The transverse energy deposited in the calorimeter in a hollow cone of $0.1 < \mathcal{R} < 0.4$ around the muon is also measured. In the $e\mu$ final state, both quantities are required to be $< 0.15 \times p_{\rm T}^{\mu}$, where $p_{\rm T}^{\mu}$ is the transverse momentum of the muon. In the $\mu\mu$ final state, the sum of the variables is required to be < 0.4 (0.5) $\times p_{\rm T}^{\mu}$ for the leading (trailing) muon. Muons are restricted to the fiducial coverage of the muon system $|\eta| < 2.0$. Muons from cosmic rays are rejected by requiring a timing criterion on the hits in the scintillator layers as well as applying restrictions on the position of the muon track with respect to the selected primary vertex.

In all final states, two leptons originating from the same primary vertex are required to be of opposite charge. Muons must have $p_T^{\mu} > 10$ GeV whereas electrons are required to have $p_{\rm T}^{e} > 15$ GeV. In the $\mu\mu$ final state one of the two muons is required to have $p_{\mathrm{T}}^{\mu} > 15$ GeV. In addition, the dilepton invariant mass is required to exceed 15 GeV. For the dimuon final state the number of jets with transverse energy $E_{\mathrm{T}} > 15$ GeV is required to be $n_{\mathrm{jet}} < 2$ where jets are reconstructed in the calorimeter with a cone of radius $\mathcal{R} = 0.5$. Both muons must be separated from the nearest jet by $\Delta\mathcal{R} > 0.1$. This stage of the analysis is referred to as "pre-selection".

At this stage, the background is dominated by Z/γ^* production. In the ee and $e\mu$ final states this background is suppressed by requiring missing transverse energy $\not{E}_T > 20$ GeV. Events are further removed if the $\not{E}_T$ could have been produced by a mis-measurement of jet energies. A scaled $\not{E}_T$ variable, $\not{E}_T^{\mathrm{Scaled}}$, is used for this purpose. The jet transverse energy resolution is approximated by $\Delta E^{\mathrm{jet}} \cdot \sin\theta^{\mathrm{jet}}$ where ΔE^{jet} is proportional to $\sqrt{E^{\mathrm{jet}}}$. The opening angle $\Delta\phi\,(\mathrm{jet}, \not{E}_T)$ between this projected energy fluctuation and the missing transverse energy provides a measure of the contribution of the jet to the missing transverse energy. The scaled missing transverse energy is defined as:

$$\not{E}_T^{\mathrm{Scaled}} = \frac{\not{E}_T}{\sqrt{\sum_{\mathrm{jets}} \left(\Delta E^{\mathrm{jet}} \cdot \sin\theta^{\mathrm{jet}} \cdot \cos\Delta\phi\,(\mathrm{jet}, \not{E}_T)\right)^2}}. \tag{1}$$

To suppress background where $\not{E}_T$ is coming from mis-measured lepton energy we apply a requirement on the minimal transverse mass M_T^{min}, which is the the smallest of the two transverse masses M_T built out of the momentum of either of the two leptons and $\not{E}_T$, with M_T defined as

$$M_T(l, \not{E}_T) = \sqrt{2 p_T^l \not{E}_T\,(1 - \cos\Delta\phi(l, \not{E}_T))}. \tag{2}$$

Z/γ^* boson and multijet events are rejected with a cut on the opening angle $\Delta\phi_{\ell\ell}$, since most of the background decays are back-to-back. This is not the case for Higgs boson decays because of the spin correlations from the scalar decay.

In the $\mu\mu$ channel the three selection cuts on $\not{E}_T$, $\not{E}_T^{\mathrm{Scaled}}$ and M_T^{min} are replaced by a single requirement $\not{E}_T > 20$ GeV for the events with 1 reconstructed jet or $p_{\mathrm{T}}^{\mu\mu} > 20$ GeV for events without reconstructed jets, where $p_{\mathrm{T}}^{\mu\mu}$ is the total transverse momentum of the muon pair. This different event selection is justified by the fact that in dimuon events without high E_{T} jets the missing transverse momentum is due exclusively to the difference in energy depositions of the two muons in the calorimeter and to low energy clusters in the calorimeter. The tails of the distributions of these quantities are not sufficiently well simulated at the level required by the available statistics of Z events. While the requirements applied in the $\mu\mu$ channel result in a smaller rejection of the background from Z/γ^* events, they have the advantage of being applied to quantities which are well described by the MC simulation.

Some selections are final-state dependent and optimized to further suppress contributions from Z/γ^*, diboson (WW, WZ, ZZ), $W(\to \ell\nu)$+jets, and multijet backgrounds. Table I shows the selection criteria used for the three different channels. Figure 1 shows the dilepton invariant mass and $\not{E}_T$ distributions in data, backgrounds, and signal at the pre-selection level for all three channels. The left column of Figure 2 shows the $\Delta\phi(\ell,\ell)$ distribution after the final selection for all three channels. As can be seen the simulation is in good agreement with data. Table II shows the number of expected and observed events after pre-selection and final selections for all three channels.

V. MULTIVARIATE DISCRIMINANTS

To improve the separation of signal from background, an artificial neural network (NN) is used in each of the three dilepton channels. The NNs were trained using approximately half of the background and signal events, the rest being used to test the networks' performance and to compare with data. A separate NN is trained for each Higgs boson mass tested. A weighted sum of all backgrounds was used during training.

A list of input variables was derived based on the separation power of the various distributions for each of the three channels. Those variables can be divided into three classes, lepton variables, event kinematics and angular variables. The NN input variables for the three channels are listed in Table III. The NN is applied to all events passing the final selection requirements described in Section IV. All the NN input variables show agreement between the sum of the MC backgrounds and the data after the selection cuts. The NN output for $m_{\mathrm{H}} = 165$ GeV is displayed in the right column of Figure 2 for all three channels.

		Final state	$e\mu$	ee	$\mu\mu$
Cut 0	Pre-selection		lepton ID, leptons with opposite charge and $p_T^\mu > 10$ GeV and $p_T^e > 15$ GeV invariant mass $M_{\ell\ell} > 15$ GeV $\mu\mu$: $n_{\rm jet} < 2$ for $p_{\rm T}^{\rm jet} > 15$ GeV, $\Delta\mathcal{R}(\mu,{\rm jet}) > 0.1$ and $p_T^\mu > 15$ GeV for the leading μ		
Cut 1	Missing Transverse Energy $\not\!\!E_T$ (GeV)		> 20	> 20	
Cut 2	$\not\!\!E_T^{\rm Scaled}$		> 6	> 6	
Cut 3	M_T^{min} $(\ell, \not\!\!E_T)$ (GeV)		> 20	> 30	
Cut 4	$p_{\rm T}^{\mu\mu}$ (GeV) for $n_{\rm jet} = 0$				> 20
	$\not\!\!E_T$ (GeV) for $n_{\rm jet} = 1$				> 20
Cut 5	$\Delta\phi(\ell, \ell)$		< 2.0	< 2.0	< 2.5

TABLE I: Summary of the selection criteria for the three final states (blank entries indicate that no requirement is applied on that quantity for the specific channel).

	ee pre-selection	ee final	$e\mu$ pre-selection	$e\mu$ final	$\mu\mu$ pre-selection	$\mu\mu$ final
$Z \to ee$	218695 ± 704	108 ± 14	280.6 ± 3.3	$0.0^{+0.1}_{-0.0}$	–	–
$Z \to \mu\mu$	–	–	274.6 ± 0.9	5.8 ± 0.1	235670 ± 158	3921 ± 22
$Z \to \tau\tau$	1135 ± 16	1.4 ± 0.5	3260 ± 3	7.3 ± 0.1	1735 ± 10	66 ± 2
$t\bar{t}$	131.4 ± 1.4	39.9 ± 0.8	272.0 ± 0.3	82.5 ± 0.2	19.93 ± 0.05	12.55 ± 0.04
W+jets	241 ± 5	98 ± 3	183 ± 4	78.6 ± 2.8	214 ± 7	134 ± 5
WW	172.2 ± 2.6	66.8 ± 1.6	421.2 ± 0.1	154.7 ± 0.1	159.0 ± 0.3	92.8 ± 0.3
WZ	112.5 ± 0.2	9.68 ± 0.05	20.5 ± 0.1	6.6 ± 0.1	47.3 ± 0.5	19.4 ± 0.3
ZZ	98.2 ± 0.2	7.68 ± 0.07	5.3 ± 0.1	0.60 ± 0.01	40.5 ± 0.2	15.1 ± 0.1
Multijet	1351 ± 55	$1.7^{+2.0}_{-1.7}$	279 ± 168	$1.1^{+9.6}_{-1.1}$	386 ± 20	64 ± 8
Signal ($M_H = 165$ GeV)	9.45 ± 0.01	6.13 ± 0.01	17.1 ± 0.01	12.2 ± 0.1	5.43 ± 0.01	4.85 ± 0.01
Total Background	221937 ± 707	332 ± 15	4995 ± 168	337 ± 10	238272 ± 159	4325 ± 24
Data	221530	336	4995	329	239923	4084

TABLE II: Expected and observed number of events in each channel after pre-selection and final selections (the NN input stage). Statistical uncertainties in the expected yields are shown for all backgrounds whereas the systematic uncertainty is shown for the multijet background.

NN Analysis Variables	
p_T of leading lepton	$p_T(\ell_1)$
p_T of trailing lepton	$p_T(\ell_2)$
Minimum of both lepton qualities	$\min(q_{\ell 1}, q_{\ell 2})$
Vector sum of the transverse momenta of the leptons:	$p_T(\ell_1) + p_T(\ell_2)$
Scalar sum of the transverse momenta of the jets:	$H_T = \sum_i \lvert p_T({\rm jet}_i)\rvert$
Invariant mass of both leptons	$M_{\rm inv}(\ell_1, \ell_2)$
Minimal transverse mass of one lepton and $\not\!\!E_T$	M_T^{min}
Missing transverse energy	$\not\!\!E_T$
Scalar transverse energy	$E_T^{\rm scalar}$
Azimuthal angle between selected leptons	$\Delta\phi(\ell_1, \ell_2)$
Solid angle between selected leptons ($e\mu$ only)	$\Delta\Theta(\ell_1, \ell_2)$
ΔR between selected leptons ($e\mu$ only)	$\Delta R(\ell_1, \ell_2)$
Azimuthal angle between leading lepton and $\not\!\!E_T$	$\Delta\phi(\not\!\!E_T, \ell_1)$
Azimuthal angle between trailing lepton and $\not\!\!E_T$	$\Delta\phi(\not\!\!E_T, \ell_2)$

TABLE III: Input variables for the NN.

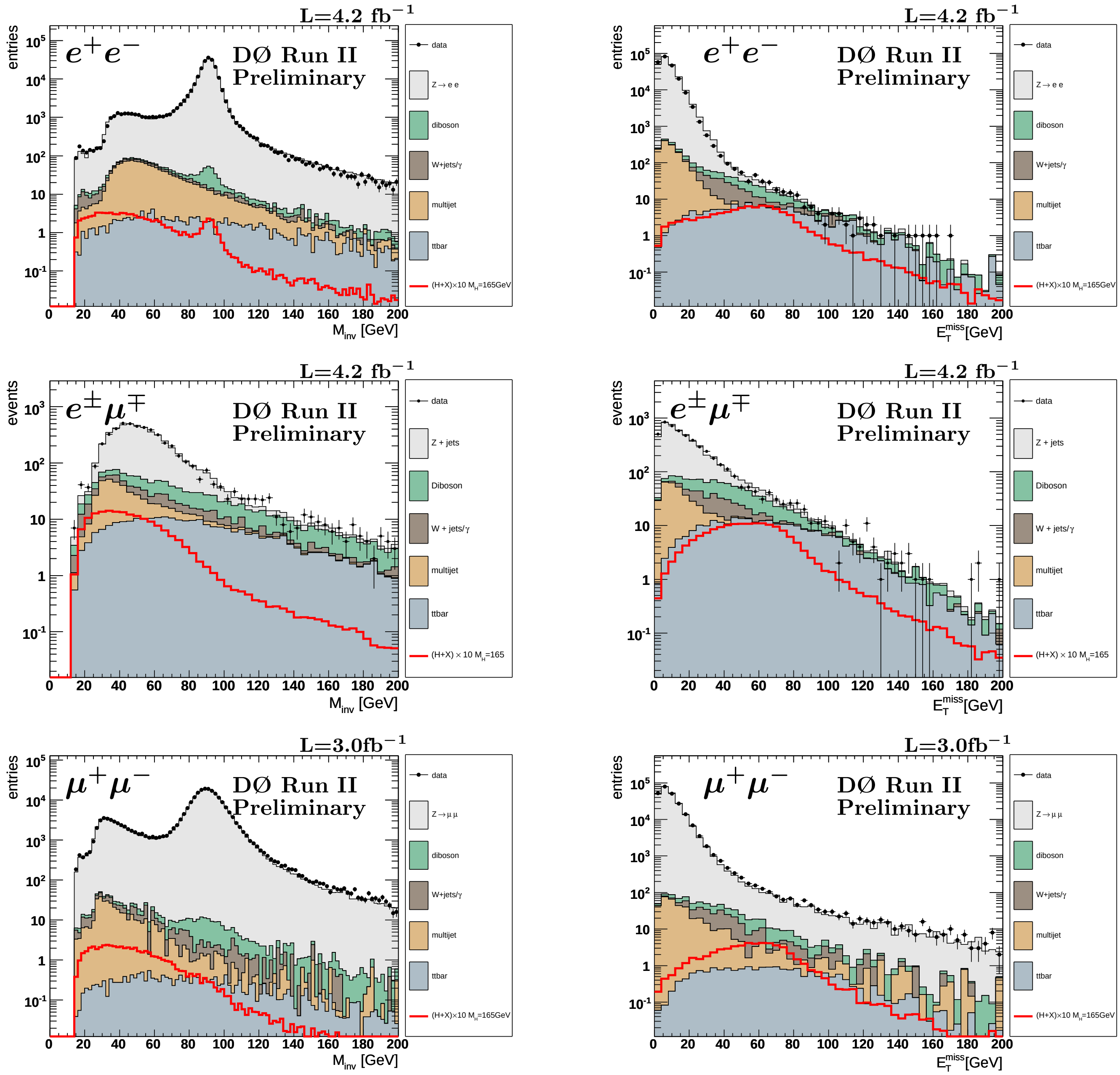

FIG. 1: Distributions of $\ell^+\ell^-$ mass (left) and $\not\!\!E_T$ (right) for data (points with error bars), background simulation (histograms, complemented with the QCD expectation) and signal expectation times 10 for $M_H = 165$ GeV (solid line) for the three different channels after pre-selection.

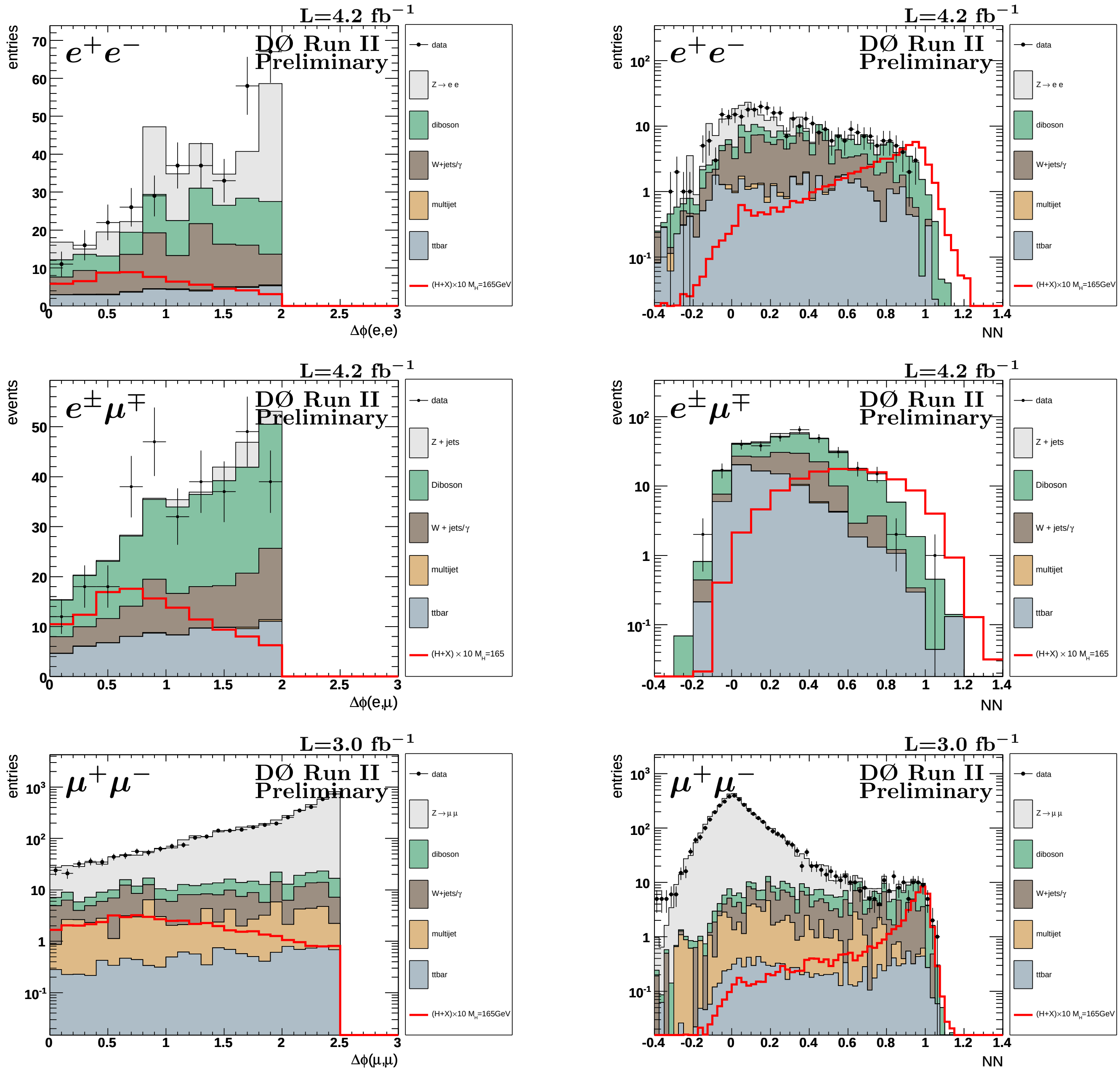

FIG. 2: Distribution of $\Delta\phi(\ell^+,\ell^-)$ (left) and the neural net output variable (right) after all selection criteria are applied for the three different channels.

VI. RESULTS AND SUMMARY

The estimates for the expected number of background and signal events depend on numerous factors that each introduce a systematic uncertainty. We consider the effect of systematic uncertainties both on the normalization and on the shape of the neural network's differential distributions for signal and backgrounds. The following sources of systematic uncertainties affecting only the normalization of the backgrounds and of the signal efficiency have been considered: lepton reconstruction efficiencies (2.5-4%), lepton momentum calibration (2-8%), theoretical cross section (diboson 7%, $t\bar{t}$ 10%, W+jet 20%, Z+jet 6%, Higgs signal 10%), and modeling of multijet background (2-20%), luminosity (6.1%). For the following source of systematic uncertainties we consider also the impact on the shape the NN distributions: jet reconstruction efficiency (6-18%), jet energy scale calibration (3-17%), jet energy resolution (2%), modeling of $p_{\mathrm{T}}(WW)$, $p_{\mathrm{T}}(H)$, and $p_{\mathrm{T}}(Z)$ (1-5%). The systematic uncertainty on the p_{T} modeling is determined by comparing the p_{T} distributions of Pythia, Sherpa, and MC@NLO. The Sherpa and MC@NLO event generators agree well with each other and generate harder p_{T} spectra than Pythia (see also [23]). The total uncertainty on the background level is approximately 13% and for the signal efficiency it is 10%.

After all selection cuts, the NN output distributions in data agree within uncertainties with the expected backgrounds as shown in Figure 2. Thus the NN output distributions are used to set limits on the Higgs boson inclusive production cross section $\sigma(p\overline{p} \to H + X)$ assuming SM values for the branching ratios. We calculate limits for each channel and all three channels combined, using a modified frequentist method, the CLs method, with a log-likelihood ratio (LLR) test statistic [24]. To minimize the degrading effects of systematics on the search sensitivity, the individual background contributions are fitted to the data observation by maximizing a profile likelihood function for each hypothesis [25]. Figures 3 and 4 show the result of the constrained fit for the combination of all three channels before and after background subtraction. Table IV presents expected and observed upper limits at 95% C.L. for $\sigma(p\overline{p} \to H + X)$ relative to that expected in the SM for each of the three final states and for their combination for each Higgs boson mass considered.

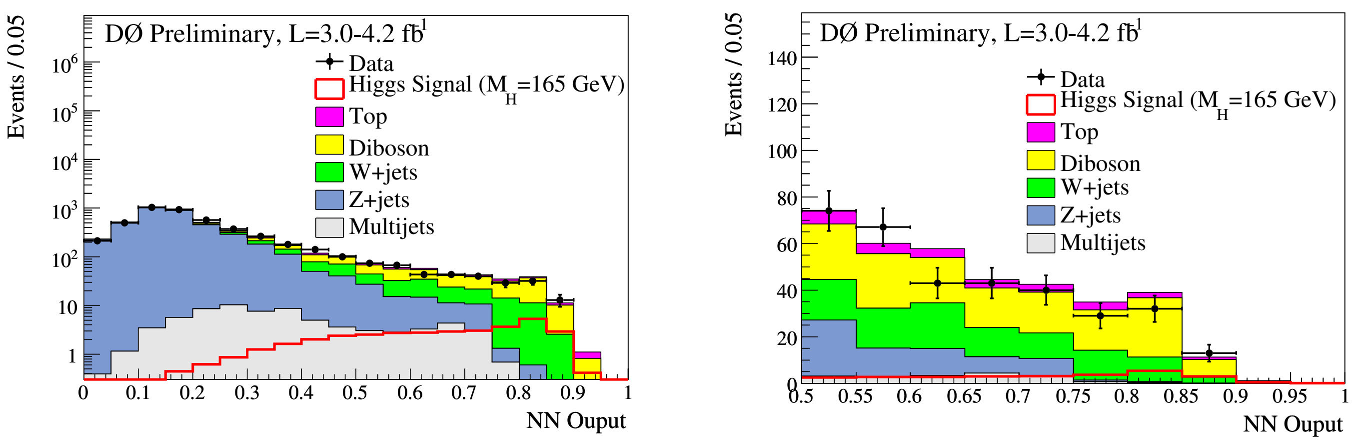

FIG. 3: Data, standard model signal expectation and backgrounds as a function of the neural net output variable. The expected standard model signal for a Higgs boson mass of $M_H = 165$ GeV is shown by the red histogram. The neural net output is shown in logarithmic scale (left) and in linear scale for the high NN region (right).

Figure 5 shows the expected and observed limits for $\sigma(p\overline{p} \to H + X)$ relative to the SM for the different Higgs boson masses and the LLR distribution for the 3.0–4.2 fb^{-1} of Run II data. Figure 6 shows the confidence level for the exclusion of the cross section i $\sigma(p\overline{p} \to H + X)$ in units of the SM cross section for all the three channels combined as a function of the Higgs boson mass. So far, no region of the SM Higgs boson mass range can be excluded and no significant excess of events is observed in data. However using the data of DØ alone the sensitivity of the current analysis has reached an expected confidence level for the exclusion of the SM cross section for an Higgs boson with $M_H \approx 160$ GeV close to 80%. With increased integrated luminosity it will be possible to exclude the presence of a Higgs boson with masses in this range.

[1] R. Barate *et al.*, Phys. Lett. B **565**, 61 (2003).

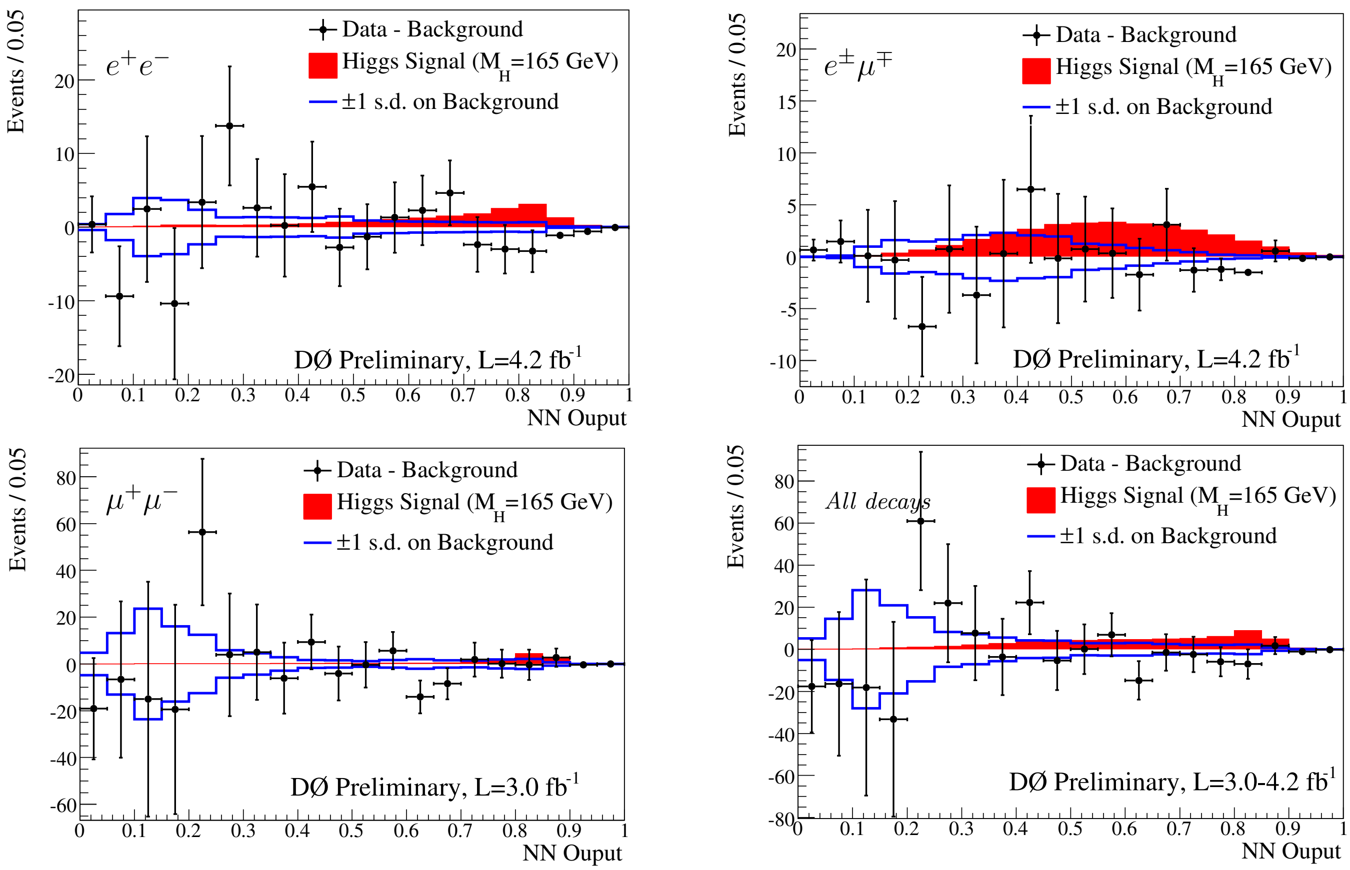

FIG. 4: Data and SM signal expectation after background subtraction as a function of the neural net output variable. The background resulting from the constrained fit using the signal plus background hypothesis is subtracted. The standard model signal expectation is shown by the red histogram. The constrained total systematic uncertainty is shown by the blue line.

TABLE IV: Expected and observed upper limits at 95% C.L. for $\sigma(p\overline{p} \to H + X)$ relative to the SM for e^+e^-, $e\mu$, and $\mu^+\mu^-$ final states in Run II and their combination for different Higgs boson masses (M_H).

M_H=	115	120	125	130	135	140	145	150	155	160	165	170	175	180	185	190	195	200
ee (exp.)	44	28	18	13	9.9	8.0	6.1	5.9	4.7	3.3	3.3	3.6	4.4	4.9	7.0	8.2	9.9	10
ee (obs.)	30	19	16	13	9.1	8.0	6.9	5.9	3.2	3.0	2.2	3.0	3.1	3.6	6.7	5.8	7.3	8.4
$e\mu$ (exp.)	40	23	19	11	11	8.5	7.7	4.3	3.5	2.6	2.3	2.7	3.2	3.8	5.1	6.4	7.6	8.4
$e\mu$ (obs.)	48	34	24	15	11	7.6	10	5.0	3.8	2.3	1.8	1.9	2.2	2.5	3.6	4.0	4.5	5.6
$\mu\mu$ (exp.)	94	36	23	16	16	11	10	8.2	7.6	6.4	5.7	5.9	7.7	9.2	12	14	16	19
$\mu\mu$ (obs.)	104	25	20	15	11	14	10	10	7.5	7.2	6.4	4.3	6.9	6.9	9.0	14	10	14
Run II (exp.)	23	13	9.6	6.3	5.6	4.7	4.0	2.9	2.4	1.8	1.7	2.0	2.4	2.9	4.0	4.8	5.8	6.7
Run II (obs.)	28	13	13	7.8	5.5	6.2	5.6	4.0	2.3	1.7	1.3	1.3	1.7	1.6	2.9	2.8	3.1	3.7

[2] The LEP Electroweak Working Group, the Tevatron Electroweak Working Group, *Precision Electroweak Measurements and Constraints on the Standard Model*, arXiv:0811.4682 [hep-ex].

[3] T. Han, A. Turcot, R-J. Zhang, Phys. Rev. D **59**, 093001 (1999).

[4] M. Carena *et al.* [Higgs Working Group Collaboration], "Report of the Tevatron Higgs working group", hep-ph/0010338.

[5] DØ Collaboration, V. Abazov *et al.*, Phys. Rev. Lett. 96, 011801 (2006).

[6] DØ Collaboration, DØNote 5757, *Search for the Higgs Boson in $H \to WW^{(*)} \to \ell\ell'$ ($\ell, \ell' = e, \mu$) decays with 3.0 fb^{-1} at DØ in Run II*, (July 2008).

[7] DØ Collaboration, V. Abazov *et al.*, Nucl. Instrum. Methods Phys. Res. A. **565**, 463 (2006).

[8] T. Andeen *et al.*, Report. No. FERMILAB–TM–2365 (2007).

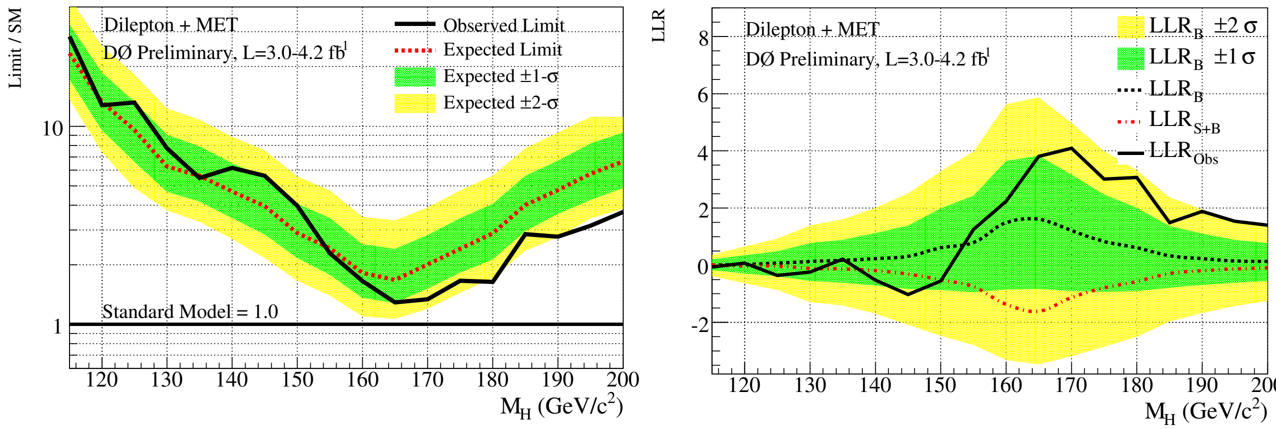

FIG. 5: Excluded cross section ($\sigma(p\overline{p} \to H + X)$) at 95% C.L. in units of the SM cross section (left) and LLR (right) for all three channels combined as a function of the Higgs boson mass, using 3.0–4.2 fb^{-1} of Run II data.

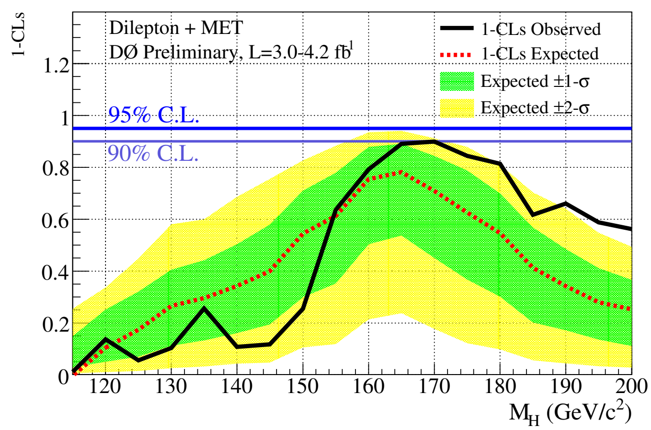

FIG. 6: Confidence level for the exclusion of the cross section $\sigma(p\overline{p} \to H + X)$ in units of the SM cross section for all the three channels combined as a function of the Higgs boson mass, using 3.0–4.2 fb^{-1} of Run II data.

[9] T. Sjöstrand *et al.*, Comp. Phys. Comm. **135**, 238 (2001), we use version 6.323 or later.
[10] J. Pumplin et al., JHEP **07**, 012 (2002).
[11] R. Brun and F. Carminati, CERN Program Library Long Writeup W5013, 1993 (unpublished).
[12] S. Catani, D. de Florian, M. Grazzini and P. Nason, JHEP **0307**, 028 (2003).
[13] K.A. Assamagan *et al.*, [Higgs Working Group Collaboration], arXiv:hep-ph/0406152.
[14] U. Aglietti, R. Bonciani, G. Degrassi, A. Vicini, arXiv:hep-ph/0610033.
[15] C. Anastasiou, R. Boughezal, F. Petriello, arXiv:0811.3458 [hep-ph].
[16] T. Gleisberg, S. Höche, F. Krauss, A. Schälicke, S. Schumann and J. Winter, JHEP **0402**, 056 (2004).
[17] M.L. Mangano, M. Moretti, F. Piccinini, R. Pittau, A. Polosa, JHEP **0307**, 001 (2003), we use version 2.11.
[18] R. Hamberg, W.L. van Neerven, and T. Matsuura, Nucl. Phys. **B359**, 343 (1991) [Erratum-ibid. **B644**, 403 (2002)].
[19] DØ Collaboration, V. Abazov *et al.*, Phys. Rev. Lett. 100, 102002 (2008)
[20] S. Moch, P. Uwer, Phys. Rev. D**78**, 034003 (2008), we use $\sigma(t\bar{t}) = 7.88$ pb.
[21] J. M. Campbell and R. K. Ellis, Phys. Rev. D **60**, 113006 (1999), we use $\sigma(WW) = 11.66$ pb, $\sigma(WZ) = 3.45$ pb and $\sigma(ZZ) = 1.37$ pb.
[22] T. Binoth, M. Ciccoli, N. Kauer, M. Krämer, JHEP **0503**, 065 (2005), JHEP **0612**, 046 (2006).
[23] T. Gleisberg, F. Krauss, A. Schälicke, S. Schumann and J. C. Winter, Phys. Rev. D **72**, 034028 (2005).
[24] T. Junk, Nucl. Instrum. Methods Phys. Res. A. **434**, 435 (1999). A. Read, CERN 2000-005 (30 May 2000).
[25] W. Fisher, FERMILAB-TM-2386-E.